Activating a Cu/ZnO:Al Catalyst – much more than Reduction: Decomposition, Self-doping and Polymorphism

Elias Frei[a]*, Abhijeet Gaur[b], Henning Lichtenberg[b], Christian Heine[a], Matthias Friedrich[a], Mark Greiner[c], Thomas Lunkenbein[a], Jan-Dierk Grunwaldt[b], Robert Schlögl[a,c]

Abstract: The activation of Cu/ZnO-based catalysts before their application is a key step and sensitive process enabling the development of the entire catalytic potential. Here, we report on a complementary (soft and hard) *in-situ* X-ray absorption spectroscopy (XAS) study investigating in detail the changes of a Cu/ZnO:Al catalyst upon thermal treatment in reducing atmosphere (10% H_2) at ambient pressure. The spectroscopic features of Cu, Zn and Al are investigated. Beyond the reduction event of the Cu moieties, the role of high temperature carbonate and the Al-dopant is discussed up to the consequences for the ZnO polymorphism. The stability of the observed effects and thus their catalytic relevance are validated by *operando* XAS under reverse water gas-shift conditions.

Cu/ZnO-based catalysts are applied in CO and CO_2 hydrogenation reactions like methanol synthesis and reverse water gas-shift (rWGS) reaction since decades.[1] Numerous thorough investigations on the synthesis of the precursor and the influence of the synthesis parameters are conducted.[2] Also the thermokinetic analysis of the subsequent calcination step to the oxidic precatalyst is known, including a discussion of the possible role of high temperature carbonates (HT-CO_3) in catalysis.[3] Besides, some studies discuss the state of the activated catalyst before and after catalytic testing.[4] In addition, some studies report on oxygen deficient ZnO_{1-x} phases and different kinds of ZnO morphologies as well as the role of Al as dopant of the ZnO.[5] Based on a precise control of the synthesis conditions, structure-activity correlations are extracted and various active site models are proposed.[6] However, in all of these references the CuZnO-based catalysts have to be activated or reduced. Generally, the process of activation is regarded equivalent to the reduction of the Cu-oxides to Cu metal[7] and the fate of Zn and Al is neglected.

In this work, we report on detailed *in-situ* investigations during the activation process of a Cu/ZnO:Al (in atom-% 69Cu / 29Zn / 2Al, XRF Table S2) catalyst by means of ambient pressure X-ray absorption near edge spectroscopy (XANES) and extended X-ray absorption fine structure spectroscopy (EXAFS) at the L-edge of Cu/Zn and the K-edge of Cu/Zn/Al. The gas atmosphere is analyzed by online mass spectrometry. In addition, *operando* XANES and EXAFS measurements are performed under rWGS conditions. The synthesis protocol is described briefly in the supporting information (SI). In previous studies an analogously prepared catalyst showed very promising catalytic results.[8] XANES reference measurements are given in the SI. The structural changes of the precursor upon calcination and activation are investigated *in-situ* by powder XRD as integral method (Fig S9a-c).

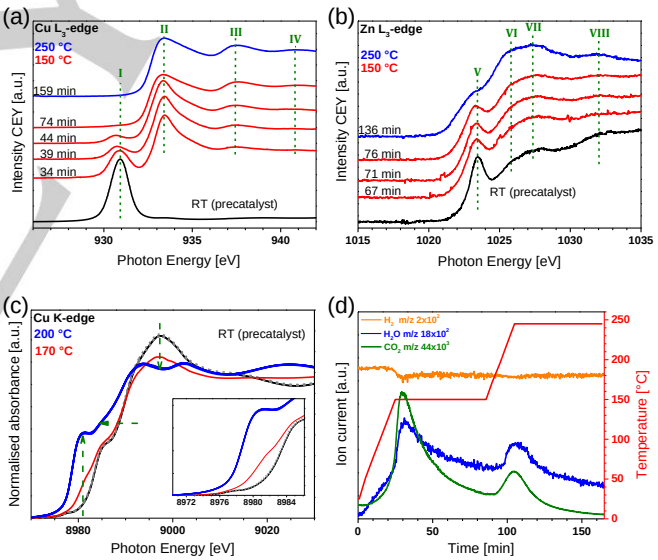

Figure 1: XANES measurements at the Cu- and Zn-edges during catalyst activation in 10% H_2/Ar at ambient pressure. The normalized spectra are shown at different temperatures and times (a)+(b). The corresponding gas analysis is given in (d). The normalised Cu K-edge XANES spectra at different temperatures in (c).

Figure 1(a) shows the XANES data of the Cu L_3-edge, a sensitive probe of the Cu oxidation state, as a function of temperature and time in 10% H_2/Ar at 980 mbar. Since the conversion electron yield (CEY) was measured, the gained information is particularly surface sensitive.[9] The precatalyst at room temperature (RT) is measured as reference (black curve). Feature-**I** at 931 eV is identified as Cu(II) as part of the oxidic CuO/ZnO:Al precatalyst (2*p* to 3*d* transition).[10] Upon heating to 150 °C feature-**I** decreases continuously and already at 150 °C and 74 min, no Cu(II) is visible anymore. Consequently the Cu(I) white-line at 150 °C increases gradually until 44 min, visible as

[a] Dr. E. Frei *, Dr. Matthias Friedrich, Dr. Christian Heine, Prof. Dr. R. Schlögl
Department of Inorganic Chemistry
Fritz-Haber Institut der Max-Plack Gesellschaft
Faradayweg 4-6, 14195, Berlin, Germany
[*] corresponding author:
E-mail: efrei@fhi-berlin.mpg.de

[b] Prof. Dr. Jan-Dierk Grunwaldt, Dr. Henning Lichtenberg, Dr. Abhijeet Gaur
Karlsruher Institut für Technologie, ITCP and IKFT
Engesserstr. 20, 76131 Karlsruhe, Germany

[c] Prof. Dr. R. Schlögl, Dr. Mark Greiner
Department of Heterogeneous Reactions
Max-Planck-Institute for Chemical Energy Conversion
Stiftstrasse 34-36, 45470 Mühlheim an der Ruhr, Germany

Supporting information for this article is given via a link at the end of the document

feature-**II** at 933.3 eV. At 150 °C and 74 min, the white-line starts to decrease again. This is explained by a decrease of transitions into the hybridization (3*d*-4*s*) induced unoccupied 3 *d*-states from Cu(I) to Cu(0) and an ongoing formation of Cu(0) metal occurs. This is accompanied by an increase of feature-**III** and -**IV** at 937.5 and 940.8 eV, respectively, which is attributed to transitions into unoccupied 4*s* states, 3*d* states with t_{2g}-(feature-**III**) and e_g-symmetry (feature-**IV**).[10-11] Between 150 °C / 74 min and 250 °C / 159 min only minor changes are visible, indicating an almost complete reduction to Cu(0) near the surface at already 150 °C. Besides, the relative intensities of the post white-line resonances (feature-**III** and -**IV**) indicate charge transfer contributions.[11] Figure S2(a)+(b) shows the change of the Cu L_3-edge at 250 °C as a function of time (blue curve in Fig. 1a shows the final state). The data are normalized to the white-line and thus relative changes, also compared to a Cu reference foil, become visible. Flattened and not well resolved features-**III** and -**IV** represent a charge transfer to the Cu metal from the metal oxide moieties (ZnO:Al).[5c, 12] This effect weakens with increasing dwell time at 250 °C and 10% H_2 in Ar at ambient pressure but still remains remarkably pronounced. For an efficient charge transfer, intimate interfacial contact (strong metal-support interaction, SMSI) is needed and prototypically described for CuZnO-based catalysts.[5a, 6a, 6d, 7a, 13].

These findings are supported by Figure 1(c) illustrating the Cu K-edge XANES spectra at different temperatures recorded at the recently installed CAT-ACT beamline[14] at the KIT synchrotron. The precatalyst shows a pre-edge at 8978 eV (1*s* to 3*d* transition) and a shoulder at 8986 eV (see inset Fig 1c). The first is attributed to Cu(II) in tetragonal environment and the latter indicates a calcination controlled Cu(II) doped ZnO in tetrahedral coordination.[15] This partly intermixed CuO-ZnO:Al interface, already present in the oxidic state and controlled by the synthesis protocol, is tentatively interpreted as prerequisite for an effective charge transfer and SMSI. The decreasing white line at 8997 eV, a shift of the shoulder at 8988 to 8984 eV and an increase at 8981 eV (see green arrows Fig. 1c) indicate a complete reduction to Cu(0) at 200 °C, also for the more bulk-like Cu-moieties.[7a] The ongoing reduction as a function of time and temperature (Fig. 1a) is also monitored by the consumption of H_2 and the formation of H_2O (Figure 1d, mass traces correspond to the measurement of the L_3-edges of Cu/Zn and the K-edge of Al in Fig. 2a). The reduction completes during heating to 250 °C (see second H_2O evolution, Fig. 1d), which is in good agreement with the XANES data of the Cu edges (Fig. 1a+c). At RT, EXAFS fitting results (Table S1 and Figure S5) give a coordination number N=3.2±0.4 for the first coordination shell (Cu-O, 1.95 Å), a typical value below N<4 for nanostructured CuO.[16] At 2.92 Å another coordination shell is fitted (N=4, fixed) and might be ascribed to a small contribution of tetrahedrally coordinated Cu in ZnO as already discussed above. At 250 °C in the reduced state, the extracted EXAFS results give a Cu-Cu coordination number of N=8.3±1.5 at 2.53 Å, which is again representative for defective nanostructured Cu moieties with an particle size estimated by EXAFS in the range of 2 nm (TEM analysis 8-9 nm[8]).[7a, 15, 17] The low coordination number and estimated particle size might be due to the initial formation of small Cu particles, a rather high Debye-Waller-factor and defective, not perfectly shaped nanoparticles. Another contribution to these low numbers might be possible alloying with Zn, observed for model catalysts at 250 °C.[7a] However, the Cu domain size determined by *in-situ* XRD measurements confirms Cu nanostructures in the lower nm regime (L_{vol}-IB = 3±0.09 nm) and the lattice parameter *a*=3.6143 Å corresponds to metallic Cu[18] as a sensitive probe for Zn incorporation (no alloying).

The Zn L_3-edge of the precatalyst in Figure 1(b) shows a pre-resonance at 1023.4 eV (feature-**V**) and three oscillations at 1025.8, 1027.3 and 1031.9 eV (feature-**VI**, **VII** and **VIII**). Feature-**V** is attributed to $Zn(CO_3)$ or other Zn(II)-salts like $ZnSO_4$ or $Zn(NO_3)_2$ and is assigned to 4*s* contributions.[19] The features-**VI**, **-VII** and **-VIII** correlate with 4*d*-transitions, while the intensity ratio between the double feature-**VI**+**VII** and -**VIII** is interpreted as an indicator for the bonding character of the Zn (the following interpretation of e.g. iconicity or binding situation is solely discussed from the perspective of Zn). A higher intensity for feature-**VIII** represents a higher ionic character of the bonding (e.g. at RT) and a more intense **VI**+**VII** double-feature more covalence (i.e. at 250 °C).[20] Further, a higher covalent character of the Zn-O bond within the ZnO leads also to stronger contributions from hybridized orbitals (O 2*p*- and Zn 3*d*-states) to the Zn L_3-edge spectrum.[21] This is in line with the continuously decreasing feature-**V** accompanied by a release of CO_2 (Fig. 1d) due to the decomposition of ionic $ZnCO_3$. The process of losing HT-CO_3 and ionicity starts at 150 °C and finishes during heating to 250 °C. It is very likely that the reduction to Cu(I) and finally Cu(0), particularly at 150 °C, also contributes to the CO_2 emission since HT-CO_3 is not exclusively attributed to the Zn-moieties. These findings imply that the so far controversially discussed role of the Cu/Zn-HT-CO_3 is related to the activation period since it decomposes completely.[3a] It might have a strong influence on the microstructure due to a slow-down of the reduction process itself and a possible control of phase separation tendencies.

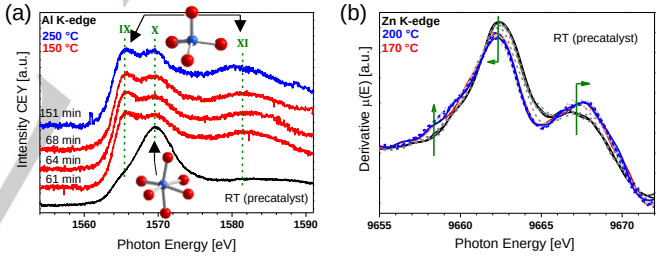

Figure 2: XANES measurements of the Al- and Zn K-edges during the catalyst activation in 10% H_2/Ar at ambient pressure. The Al K-edge is plotted as a function of time and temperature (a). Derivative Zn K-edge spectra at the Zn K-edge at different temperatures (b).

Figure 2(a) shows changes of the Al K-edge features during the activation process. The Al K-edge is a sensitive probe for the coordination environment of Al^{3+}.[22] The precatalyst at RT has a shoulder at 1565.4 eV (feature-**IX**), a main resonance at 1569.5 eV (feature-**X**) and a broad event at 1581.4 eV (feature-**XI**). The strong absorption feature-**X** represents octahedrally coordinated Al^{3+}. This might be attributed to x-ray amorphous Al_2O_3 polymorphs in the precatalyst.[23] At 150 °C in reducing atmosphere the intensity ratios change completely and feature-**IX** is the most intense one, coupled to an increase of the broad feature-**XI**. The change in the intensity ratios also represents a change of the coordination environment of Al^{3+} from octahedral to tetrahedral. This is a rather uncommon coordination for a pure alumina phase and is interpreted as a migration of the Al-cations into the structure of the tetrahedrally coordinated wurtzite ZnO. The localization of Al^{3+} on ZnO sites (Al_{Zn}) was recently confirmed by ^{27}Al-NMR (structural) and optical band gap (electronic) measurements.[5c] Here, the CuO/ZnO-Al_2O_3 precatalyst develops a kind of self-doping upon activation to

finally reach the reduced and Al-doped Cu/ZnO:Al state. The Al-dopant is an important promoter and increases the CH_3OH activity significantly.[5b] The suggested mechanism of self-doping would further explain the strongly Al-enriched surface upon activation[8] and the limited amount of Al^{3+} stabilized in ZnO without phase separation.[5b] The slightly increasing intensity of the feature-**X** at 250 °C is interpreted as an increase of octahedrally coordinated Al due to the possible formation of Al_2O_3 or $ZnAl_2O_4$ phase as a first sign of a segregation and deactivation event (i.e. γ-Al_2O_3 exhibits a defective spinel structure).[4a] This observation is supported by the slightly decreasing charge transfer from ZnO:Al to Cu metal at 250 °C (Fig. S2). Generally, the charge transfer from ZnO:Al to Cu and its accumulation at the interface might lead to an additional electrostatic stabilization of the latter and explain the higher stability compared to non-doped Cu/ZnO catalysts.[3a]

Figure 2(b) shows the derivative XANES spectra at the Zn K-edge (see corresponding XANES Zn K-edge spectra Fig. S3) monitoring the changes of the sample from a different perspective. With increasing temperature, also the shoulder of the derivative at 9658.5 eV increases and is attributed to a difference in the pre-edge region due to the increasing number of oxygen vacancies (induced by the Al self-doping) and a possible overlap of the conduction band (Zn 4*s*-, 4 *d*- and O 2*p*-states) and the Zn 3*d*-band.[24] This shoulder is also pronounced

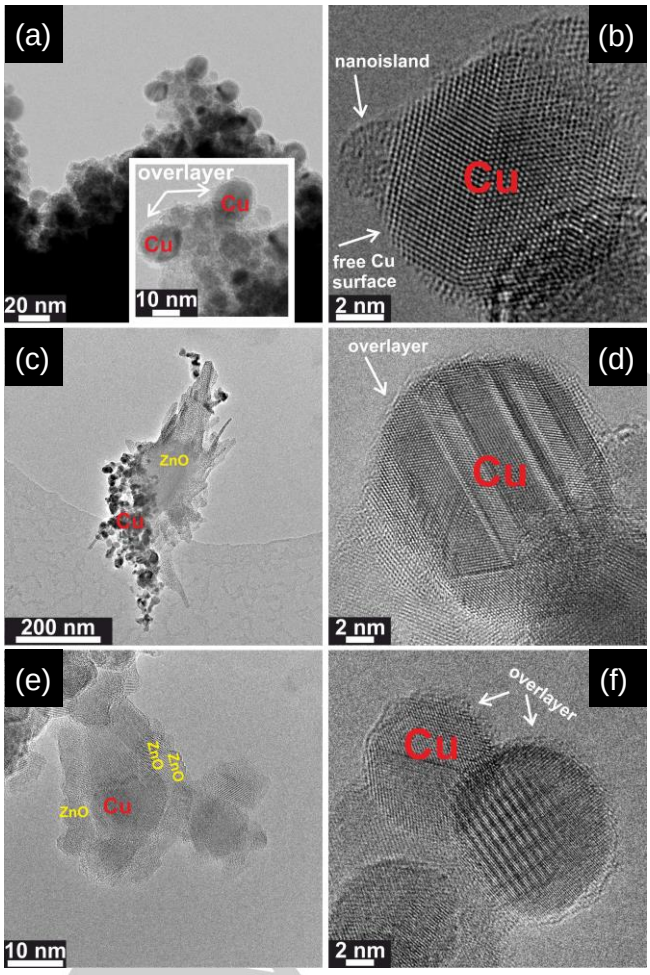

Figure 3: HRTEM investigations on the Cu/ZnO:Al catalyst activated at 250°C in 10 % H_2 in Ar (a), after 60 min at 150 °C in 10 % H_2 in Ar (b), activated at 250 °C without HT-CO_3 (c)+(d) and the binary Cu/ZnO catalyst activated at 250 °C (e)+(f). A detailed analysis of the HRTEM micrographs is presented in Figure S4.

in the derivative of the Zn K-edge of a Zn metal reference (Fig. S10a). As a consequence Zn becomes slightly more electron-rich and metallic, probably leading to an increased covalent character. This is supported by a decrease (and shift to lower photon energies) of the derivative at 9662.5 eV, attributed to the loss in ionicity due to decomposition of $ZnCO_3$ accompanied by a change in the coordination environment from in parts octahedral ($ZnCO_3$) to tetrahedral (wurtzite ZnO). The increase and shift of the resonance at 9667.5 eV to higher photon energies with increasing temperature is again a typical near edge feature of doped ZnO (ZnO asymmetry, higher covalence).[25] The slightly increasing features (9663 and 9673 eV) of the Zn K-edge as a function of time at 200 °C support the possible formation of small amounts of $ZnAl_2O_4$-spinel (Fig.S3).[24] The EXAFS fitting results of the Zn K-edge data at RT (Table S1) give an oxygen coordination at 1.94 Å of N=2.9±0.7. This low coordination number N<4 is a typical sign for nanostructured ZnO, which is further decreased upon reduction at 250 °C to N=2.6±0.7 at 1.93 Å and evidences an oxygen deficient character of ZnO.[8] This is underlined by the parallel occurrence of various types of metastable ZnO polymorphs, i.e. layered or graphitic-like ZnO (N=3, higher electron density at Zn(II-x)).[5d-f, 8] The formation mechanism of the ZnO-overlayer was so far related to the reduction process. Since the activation of a catalyst depends, besides the reduction, on manifold processes, all of these might have an impact on the polymorphism of ZnO. Figure 3(a) shows a TEM image of the activated catalysts at 250 °C with a homogeneous Cu-ZnO nanostructure and a pronounced ZnO-overlayer formation. At 150 °C the Cu particles are not yet entirely embedded or covered by ZnO (Fig. 3b). This is interpreted as the initialization state of the ZnO-overlayer formation.

To clarify the contribution of the HT-CO_3 to the ZnO-overlayer formation and self-doping process, a HT-CO_3-free precatalyst calcined at 520 °C was activated in 10 % H_2 in Ar and investigated *in-situ* with XANES (see also Table S2). Figure S7(a-c) show XANES spectra at the Cu/Zn L_3-edges and the Al K-edge. In Figure S7a no HT-CO_3 feature is identified already at RT since the pre-resonance at 1023.4 eV is absent. In addition, the covalent character of the Zn-O bonding is indicated by the double feature around 1028 eV, more intense than the feature at ~1032 eV. Figure S7b shows the stepwise reduction of Cu(II) to Cu(0) with weak post-edge oscillations, particularly at 942 eV, clearly corroborating the charge transfer contribution from the ZnO:Al (see also Fig. 1a and b).[11] The Al K-edge in Figure S7c again illustrates the change in the coordination environment of Al^{3+} from octahedral to tetrahedral, evidencing the self-doping process of ZnO:Al (Al^{3+} into ZnO) also occurring without HT-CO_3 as part of the precatalyst structure. This is in line with HR-TEM investigations showing the formation of a ZnO-overlayer created upon activation of a HT-CO_3-free sample (Fig. 3d). Furthermore, the high calcination temperatures and the absence of HT-CO_3 seem to lead to an inhomogeneous distribution of Cu- and ZnO-moieties (Fig. 3c). This would be in line with the interpretation on the impact of HT-CO_3 as species controlling the activation process and phase separation tendencies.

Figure 3(e) and 3(f) show HR-TEM images of a binary Cu/ZnO catalyst without Al. The nanostructured Cu metal is mainly embedded into a crystalline wurtzite ZnO phase (Fig. 3e). The formation of ZnO-overlayer structures is indicated in Figure 3(f), but in comparison to the ternary Cu/ZnO:Al system (Fig. 3a) underrepresented. This is tentatively interpreted as a correlation of the self-doping process of the system and the polymorphism

of ZnO upon activation, leading to a kind of push-pull mechanism when the reduction of Cu is accompanied by Al^{3+} migration into the ZnO lattice (SMSI induced push-mechanism in the binary case).

To finally judge the catalytic relevance of the discussed processes, a fresh sample was again reduced at ambient pressure in 10 % H_2 in Ar with a heating rate of 5 °C/min and a dwell time of 30 min (Fig. 4). To extract the changes of the Cu/Zn L_3-edges and Al K-edge occurring upon switching the gas feed from reducing to rWGS mixture (5 % H_2 / 5 % CO_2 in Ar), all edges were measured before applying the rWGS reaction conditions and after reaching a steady-state performance. Figure 4(d) monitors changes of gas atmospheres and product formation by mass spectrometry and gas chromatography. The formation of the rWGS products H_2O and CO is clearly visible when introducing CO_2 in the feed. Already after 60 min under rWGS conditions a steady-state situation is reached without any sign of deactivation, which means the spectra measured in the following represent the catalyst in an activated state. Since the CO_2 containing gas environment decreases the signal to noise ratio, several spectra are averaged. The smoothed curves are additionally shown in Fig. S8. Figure 4(a) shows the Cu L_3-spectra. During the rWGS reaction the post-edge oscillations are slightly increased, particularly at 941 eV (see also Fig. S8a).

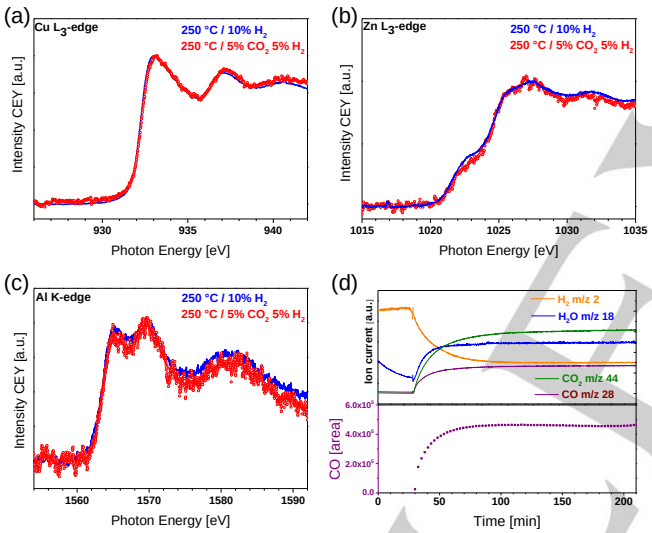

Figure 4: XANES measurements of the Cu L_3-edge (a), Zn L_3-edge (b), Al K-edge (c) before and after applying the rWGS reaction at WHSV of 24000 ml/g. Product analysis with MS (not corrected for fragmentation contributions) and GC is shown in (d).

The Zn L_3-edge (Fig. 4b and S8b) shows a decrease of the shoulder at 1023.5 eV and the post-resonance (1033-1034 eV) with respect to the double feature at 1026-1027 eV. The changes of the Al K-edge under rWGS conditions are also small but visible (Fig. 4c). With respect to the resonance at 1570 eV (octahedral coordination), the other features at 1565 eV and 1582 eV, representing tetrahedral coordination, are slightly decreased. All changes of the activated catalyst before and after the rWGS reaction in steady-state are rather small, however, they point in the same direction: a first sign of restructuring and recrystallization (loss of charge transfer from ZnO:Al to Cu, more wurtzite-like ZnO and less Al-dopant in ZnO). This means that after the activation, a kinetically stabilized high energy state of the ternary catalyst is created. Phase transition at the surface of the catalyst, induced by the chemical potential of the gas phase, may initialize a deactivation process governed by structural changes.[4a] Figure S6 and S10 show XANES spectra of the Cu K-edge and Zn K-edge under rWGS conditions at 250 °C. The Cu-signals observed after reduction are found to be stable under these conditions, which is in line with the findings above (Fig. S6). The derivatives of the Zn K-edges show small differences (Fig. S10b) attributed to a loss of oxygen vacancies (decrease at 9658.5 eV) and an increased covalence (shift to higher photon energies at 9662.5 and 9667.5 eV). This interpretation matches the results discussed in Fig. 4 (Cu/Zn L-edge and Al K-edge) evidencing, a rather stable character of Cu, but Zn:Al-moieties which change slightly under rWGS conditions. However, even with the surface sensitive XAFS measurements, the changes are at the limit of interpretability and a clear statement for the need of sensitive *in-situ/operando* instruments.

Another point of discussion is the layered metastable ZnO polymorph. In the available literature, this phenomenon is rarely identified and discussed. This means that (i) a reduced ternary catalyst was not often analyzed by suitable means to identify a minority phase next to Cu. (ii) The investigated catalysts were different in composition, i.e. in terms of the Al-content used for the synthesis (here: 3 at-%). Generally, the amount of Al in the industrially relevant catalyst is rather in the range of 5-10 at-%.[26] Since we identified a possible push-pull mechanism during the self-doping of ZnO as a trigger for the overlayer formation, this process might be different/absent if higher Al-contents are selected and the formation of $ZnAl_2O_4$ spinel structures are favored. However, the intimate contact of the different metal oxides is already visible in the precatalyst state. It seems that a proper activation process finally leads to an optimized interfacial contact of Cu metal and the metal oxide moieties (here: ZnO:Al) and, independent of the ZnO polymorph, the first loss in activity (formation phase) generally observed after activating a Cu/ZnO-based catalyst is due to a reduced interfacial contact by the mobility of ZnO-containing phases.

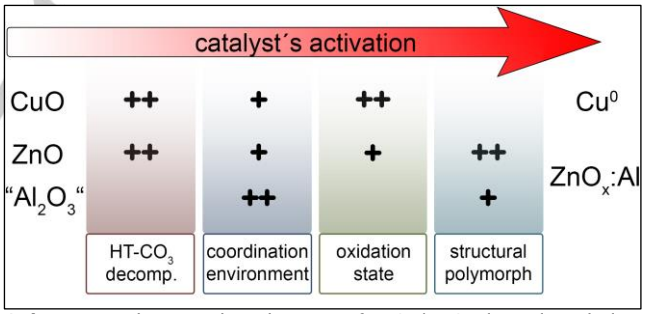

Scheme 1: The occuring changes of a Cu/ZnO:Al catalyst during its activation. The empty space symbols a negligible effect, double (++) a pronounced contribution.

In summary, we report on the intriguing processes during the activation period of a Cu/ZnO:Al catalyst, as illustratively visualized in Scheme 1. Besides the consecutive reduction of Cu(II)►Cu(I)►Cu(0), manifold other phenomena occur. The CO_2 emission at already 150 °C and the Zn L_3-edge spectra show the loss of the HT-CO_3 fractions still present after mild calcination (330 °C). The Cu K-edge spectra and EXAFS fitting results indicate a Cu(II) doping of ZnO related to calcination, as prerequisite for an intimate interfacial contact in the activated catalyst. Moreover, the coordination environment of Al changes from octahedral to tetrahedral, likely as part of a self-doping process (Al^{3+} into ZnO), enabling a charge transfer from ZnO:Al to Cu. This process is decoupled from the HT-CO_3 decomposition, since the coordination switch occurs also in a HT-CO_3-free sample (calcined at 520°C). It seems that the

migration of Al^{3+} into ZnO is part of a push-pull (Cu reduction) mechanism which triggers the polymorphism and formation of metastable layered ZnO moieties. The stability of these effects under rWGS conditions is validated since only small changes, which point at the mobility of the ZnO:Al part, are observed during steady-state catalysis. In conclusion, this combined ambient pressure *in-situ/operando* XAS study reveals the importance of a proper multi-event activation of Cu/ZnO-based catalysts in general. The mildest possible conditions (i.e. H_2 concentration, temperature, time) might yield to a maximum of kinetically stabilized high energy surfaces without phase separation and the most active catalyst.

Acknowledgement
KIT's synchrotron radiation source (operated by KIT-IBPT) is acknowledged for providing beamtime at the CAT-ACT beamline, in particular Dr. Tim Prüßmann and Dr. Anna Zimina (IKFT) for their help and technical support during XAS experiments.
EF acknowledges Dr. Gregor Koch and Dr. Frank Girgsdies for fruitful discussions and Dr. Leon Zwiener for graphical assistance. We would like to thank the Helmholtz-Zentrum Berlin (HZB) for providing access to the Innovative Station for In-Situ Spectroscopy (ISISS) beamline at BESSY II, and especially Dr. Michael Hävecker for experimental assistance during the beamtime.

References

[1] aG. C. Chinchen, P. J. Denny, J. R. Jennings, M. S. Spencer, K. C. Waugh, *Applied Catalysis* **1988**, *36*, 1-65; b*Energy* **1987**, *12*, 689-728; cA. G. George A. Olah, G. K. Surya Prakash *WILEY-VCH* **2011**.

[2] aE. Frei, A. Schaadt, T. Ludwig, H. Hillebrecht, I. Krossing, *ChemCatChem* **2014**, *6*, 1721-1730; bB. Bems, M. Schur, A. Dassenoy, H. Junkes, D. Herein, R. Schlögl, *Chemistry – A European Journal* **2003**, *9*, 2039-2052; cM. Behrens, R. Schlögl, *Zeitschrift für anorganische und allgemeine Chemie* **2013**, *639*, 2683-2695; dC. Baltes, S. Vukojević, F. Schüth, *Journal of Catalysis* **2008**, *258*, 334-344.

[3] aJ. Schumann, A. Tarasov, N. Thomas, R. Schlögl, M. Behrens, *Applied Catalysis A: General* **2016**, *516*, 117-126; bM. Schur, B. Bems, A. Dassenoy, I. Kassatkine, J. Urban, H. Wilmes, O. Hinrichsen, M. Muhler, R. Schlögl, *Angewandte Chemie International Edition* **2003**, *42*, 3815-3817; cA. Tarasov, J. Schumann, F. Girgsdies, N. Thomas, M. Behrens, *Thermochimica Acta* **2014**, *591*, 1-9; dS.-i. Fujita, S. Moribe, Y. Kanamori, N. Takezawa, *Reaction Kinetics and Catalysis Letters* **2000**, *70*, 11-16.

[4] aT. Lunkenbein, F. Girgsdies, T. Kandemir, N. Thomas, M. Behrens, R. Schlögl, E. Frei, *Angewandte Chemie International Edition* **2016**, *55*, 12708-12712; bM. B. Fichtl, D. Schlereth, N. Jacobsen, I. Kasatkin, J. Schumann, M. Behrens, R. Schlögl, O. Hinrichsen, *Applied Catalysis A: General* **2015**, *502*, 262-270.

[5] aM. B. Fichtl, J. Schumann, I. Kasatkin, N. Jacobsen, M. Behrens, R. Schlögl, M. Muhler, O. Hinrichsen, *Angewandte Chemie International Edition* **2014**, *53*, 7043-7047; bM. Behrens, S. Zander, P. Kurr, N. Jacobsen, J. Senker, G. Koch, T. Ressler, R. W. Fischer, R. Schlögl, *Journal of the American Chemical Society* **2013**, *135*, 6061-6068; cM. Behrens, G. Lolli, N. Muratova, I. Kasatkin, M. Hävecker, R. N. d'Alnoncourt, O. Storcheva, K. Köhler, M. Muhler, R. Schlögl, *Physical Chemistry Chemical Physics* **2013**, *15*, 1374-1381; dT. Lunkenbein, J. Schumann, M. Behrens, R. Schlögl, M. G. Willinger, *Angewandte Chemie* **2015**, *127*, 4627-4631; eV. Schott, H. Oberhofer, A. Birkner, M. Xu, Y. Wang, M. Muhler, K. Reuter, C. Wöll, *Angewandte Chemie International Edition* **2013**, *52*, 11925-11929; fJ. Schumann, J. Kröhnert, E. Frei, R. Schlögl, A. Trunschke, *Topics in Catalysis* **2017**, *60*, 1735-1743.

[6] aM. Behrens, F. Studt, I. Kasatkin, S. Kühl, M. Hävecker, F. Abild-Pedersen, S. Zander, F. Girgsdies, P. Kurr, B.-L. Kniep, M. Tovar, R. W. Fischer, J. K. Nørskov, R. Schlögl, *Science* **2012**, *336*, 893-897; bK. Klier, in *Advances in Catalysis, Vol. 31* (Eds.: D. D. Eley, H. Pines, P. B. Weisz), Academic Press, **1982**, pp. 243-313; cR. Burch, S. E. Golunski, M. S. Spencer, *Journal of the Chemical Society, Faraday Transactions* **1990**, *86*, 2683-2691; dJ. Nakamura, T. Uchijima, Y. Kanai, T. Fujitani, *Catalysis Today* **1996**, *28*, 223-230; eS. Kuld, C. Conradsen, P. G. Moses, I. Chorkendorff, J. Sehested, *Angewandte Chemie International Edition* **2014**, *53*, 5941-5945.

[7] aJ. D. Grunwaldt, A. M. Molenbroek, N. Y. Topsøe, H. Topsøe, B. S. Clausen, *Journal of Catalysis* **2000**, *194*, 452-460; bS. Kühl, A. Tarasov, S. Zander, I. Kasatkin, M. Behrens, *Chemistry – A European Journal* **2014**, *20*, 3782-3792; cS.-i. Fujita, S. Moribe, Y. Kanamori, M. Kakudate, N. Takezawa, *Applied Catalysis A: General* **2001**, *207*, 121-128.

[8] J. Schumann, T. Lunkenbein, A. Tarasov, N. Thomas, R. Schlögl, M. Behrens, *ChemCatChem* **2014**, *6*, 2889-2897.

[9] aC. Heine, M. Hävecker, E. Stotz, F. Rosowski, A. Knop-Gericke, A. Trunschke, M. Eichelbaum, R. Schlögl, *The Journal of Physical Chemistry C* **2014**, *118*, 20405-20412; bG. D. Moggridge, T. Rayment, R. M. Ormerod, M. A. Morris, R. M. Lambert, *Nature* **1992**, *358*, 658.

[10] M. Grioni, J. B. Goedkoop, R. Schoorl, F. M. F. de Groot, J. C. Fuggle, F. Schäfers, E. E. Koch, G. Rossi, J. M. Esteva, R. C. Karnatak, *Physical Review B* **1989**, *39*, 1541-1545.

[11] T. E. J. M. T. Greiner, S. Beeg, L. Zwiener, M. Scherzer, F. Girgsdies, S. Piccinin, M. Armbrüster, A. Knop-Gericke, R. Schlögl, *Nature Chemistry* **2018**, *DOI: 10.1038/s41557-018-0125-5*.

[12] I. Beinik, M. Hellström, T. N. Jensen, P. Broqvist, J. V. Lauritsen, *Nature Communications* **2015**, *6*, 8845.

[13] J. Schumann, M. Eichelbaum, T. Lunkenbein, N. Thomas, M. C. Alvarez Galvan, R. Schlögl, M. Behrens, *ACS Catalysis* **2015**, *5*, 3260-3270.

[14] A. Zimina, K. Dardenne, M. A. Denecke, D. E. Doronkin, E. Huttel, H. Lichtenberg, S. Mangold, T. Pruessmann, J. Rothe, T. Spangenberg, R. Steininger, T. Vitova, H. Geckeis, J.-D. Grunwaldt, *Review of Scientific Instruments* **2017**, *88*, 113113.

[15] L. S. Kau, K. O. Hodgson, E. I. Solomon, *Journal of the American Chemical Society* **1989**, *111*, 7103-7109.

[16] aA. Sharma, M. Varshney, J. Park, T.-K. Ha, K.-H. Chae, H.-J. Shin, *RSC Advances* **2015**, *5*, 21762-21771; bS. A. a. A. Waskowska, *J. Phys.: Condens. Matter* **1991** *3*.

[17] A. Jentys, *Physical Chemistry Chemical Physics* **1999**, *1*, 4059-4063.

[18] V. A. Lubarda, *Mechanics of Materials* **2003**, *35*, 53-68.

[19] aR. C. Moffet, Y. Desyaterik, R. J. Hopkins, A. V. Tivanski, M. K. Gilles, Y. Wang, V. Shutthanandan, L. T. Molina, R. G. Abraham, K. S. Johnson, V. Mugica, M. J. Molina, A. Laskin, K. A. Prather, *Environmental Science & Technology* **2008**, *42*, 7091-7097; bY. Kang, S. Lee, H. Sim, C. H. Sohn, W. G. Park, S. J. Song, U. K. Kim, C. S. Hwang, S. Han, D.-Y. Cho, *Journal of Materials Chemistry C* **2014**, *2*, 9196-9204; cI. Caretti, M. Yuste, R. Torres, O. Sánchez, I. Jiménez, R. Escobar Galindo, *RSC Advances* **2012**, *2*, 2696-2699.

[20] aM. Wang, F. Ren, J. Zhou, G. Cai, L. Cai, Y. Hu, D. Wang, Y. Liu, L. Guo, S. Shen, *Scientific Reports* **2015**, *5*, 12925; bR. Bhardwaj, A. Bharti, J. P. Singh, K. H. Chae, N. Goyal, S. Gautam, *Heliyon* **2018**, *4*, e00594.

[21] *Applied Physics Letters* **2004**, *85*, 3220-3222.

[22] aJ. A. van Bokhoven, A. M. J. van der Eerden, D. C. Koningsberger, *Journal of the American Chemical Society* **2003**, *125*, 7435-7442; bJ. A. van Bokhoven, D. C. Koningsberger, P. Kunkeler, H. van Bekkum, *Journal of Catalysis* **2002**, *211*, 540-547.

[23] I. Levin, D. Brandon, *Journal of the American Ceramic Society* **1998**, *81*, 1995-2012.

[24] R. Revel, D. Bazin, A.-M. Flank, *Journal of Synchrotron Radiation* **1999**, *6*, 717-718.

[25] aO. M. Ozkendir, S. Yildirimcan, A. Yuzer, K. Ocakoglu, *Progress in Natural Science: Materials International* **2016**, *26*, 347-353; bA. Kuzmin, J. Chaboy, *IUCrJ* **2014**, *1*, 571-589.

[26] P. J. A. Tijm, F. J. Waller, D. M. Brown, *Applied Catalysis A: General* **2001**, *221*, 275-282.

TOC